Estimation of the liquid-vapor spinodal from interfacial properties obtained from molecular dynamics and lattice Boltzmann simulations

A. R. Imre,[1,a)] G. Mayer,[1] G. Házi,[1] R. Rozas,[2,b)] and T. Kraska[2,a)]
[1]*Simulator Development Department, KFKI Atomic Energy Research Institute, P.O. Box 49, H-1525 Budapest, Hungary*
[2]*Institute for Physical Chemistry, University Cologne, Luxemburger Str. 116, D-50939 Köln, Germany*

(Received 26 October 2007; accepted 4 January 2008; published online 19 March 2008)

Interfacial pressure and density profiles are calculated from molecular dynamics and lattice Boltzmann simulations of a liquid film in equilibrium with its vapor. The set of local values of tangential pressure and density along an interface exhibits a van der Waals-type loop; starting from the stable vapor bulk phase one passes through metastable and unstable states to the stable liquid bulk phase. The minimum and maximum values of the profile of tangential pressure are related to the liquid and vapor spinodal states, respectively. The spinodal pressures turn out to be linearly related to the extreme values of the tangential pressure in the interface. The comparison with equations of state shows good agreement with the simulation results of the spinodals. In addition the properties of the metastable region are obtained. Based on this investigation a method is proposed for the estimation of the liquid spinodal from experimentally obtained interfacial properties. Estimations for water and helium are presented. © *2008 American Institute of Physics*.
[DOI: 10.1063/1.2837805]

I. INTRODUCTION

It is generally known that under atmospheric pressure water freezes at 273.15 K and boils at 373.15 K, showing a 100 K wide liquid region. It is less known that this is only true under equilibrium conditions. Under special conditions one can cool down water to 230 K without freezing or heat it up to 590 K and beyond without boiling,[1,2] revealing a much wider liquid phase region in the order of 360 K. These special conditions are high purity and the absence of any disturbance such as heterogeneous nucleation sites, mechanical shock, or cosmic radiation.[3] The reason why these conditions are required is the metastability of liquid water below 273.15 K and above 373.15 K. Between the regular equilibrium freezing and boiling points water is a stable liquid, while it is metastable outside of this region, i.e., it can exist for a certain period of time. This can be even several million years if no disturbance is present.[4]

The metastable region is bounded by the equilibrium curve toward the stable state region but also undercooling and overheating have a limit. Such limits beyond that liquid and vapor cannot exist are called stability limits. The origin of a stability limit can be kinetic or mechanical.[1] Kinetic stability limit means that a kinetic hindrance vanishes and phase separation becomes spontaneously in the time frame of the measurement. The kinetic stability limit appears before the mechanical stability limit is reached.[5] Here we focus on the classical mechanical stability limit, also called spinodal, which is the thermodynamic limit of stability of a homogenous phase.

The spinodal for the liquid-vapor transition can be approached either by increasing the temperature or by decreasing the pressure including negative values.[1–3] The liquid boils suddenly before one can approach the spinodal because the experimental time frame is always finite, i.e., one cannot measure without delay at the point in time of jumping into the nonstable region, and impurities acting as heterogeneous nuclei cannot be avoided completely.[3] Therefore, the experimental determination of the spinodal itself is impossible; only an upper boundary before reaching the actual spinodal can be approached. Another way to determine the classical spinodal is the straightforward calculation from the equation of state.[1–3,5,6] The problem is that most equations of state are constructed to describe the behavior in the stable liquid region and therefore extrapolation into the deep metastable region may be inaccurate. While such estimation of spinodals is reasonable for some, typically simple substances using suitable equations of state,[5] it can be inaccurate for complicated substances. For example, the liquid spinodal pressure of water at room temperature is given between −200 and −400 MPa depending on the chosen equation on state.[2] This difference is even larger at lower temperature.

In this paper we examine with simulations the relation between the local extreme values of the tangential pressure along an interface and the spinodal pressures. The relation involves a factor, which has a geometrical origin. Based on this relation the spinodal pressure of two liquids is estimated from experimental interfacial thickness and surface tension. The approach is investigated with two simulation methods in order to have a wider background for discussion. Furthermore, two completely different equations of state for the Lennard–Jones fluid taken from the literature are included in this analysis. Also, experimental results from the literature

[a)]Authors to whom correspondence should be addressed. Electronic addresses: imre@aeki.kfki.hu and t.kraska@uni-koeln.de.
[b)]Present address: Institut für Materialphysik im Weltraum, Deutsches Zentrum für Luft- und Raumfahrt, D-51170 Köln, Germany.

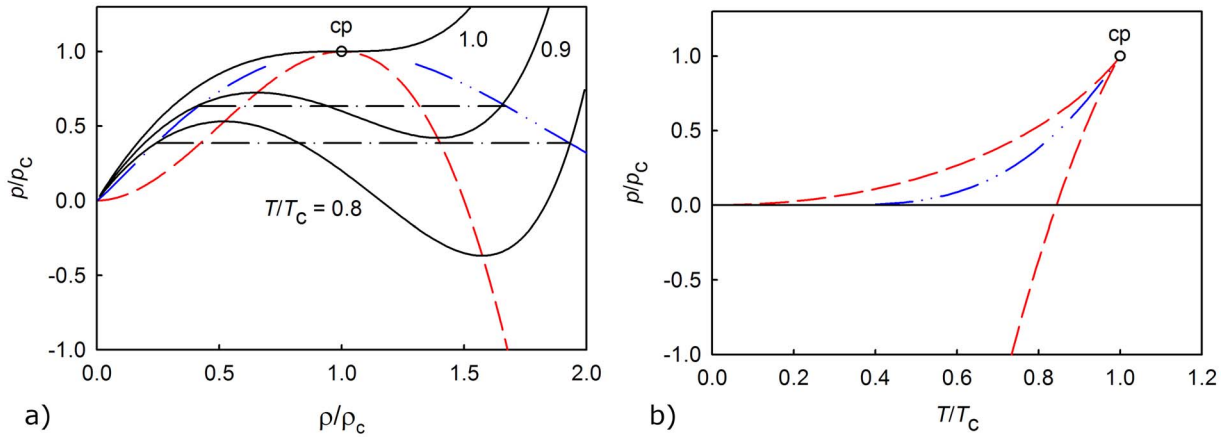

FIG. 1. (Color online) (a) Pressure-density projection of the phase diagram of a pure substance calculated with the van der Waals equation of state. Solid curves: isotherms; dash-dot-doted: binodal; dashed curve: spinodal, dot-dashed lines: Maxwell construction; cp: critical point. (b) Pressure-temperature projection of (a). Legend as in (a).

for water and helium, which are the two liquids with the most extensive set of spinodal estimations, are analyzed. The comparison of the results obtained from molecular and mesoscopic simulations, from equations of state, and from experimental data gives a consistent picture of the spinodal and exhibits largely quantitative agreement.

In Fig. 1(a) isotherms calculated with the van der Waals equation of state are illustrated, describing the density dependence of the pressure at constant temperature. The dash-dotted lines connect the stable liquid and stable vapor phases in equilibrium. Between these two points, one can see two extremes. Between these two extremes, the compressibility would be negative, which is an unphysical state violating the mechanical stability criterion,[1]

$$-\left(\frac{\partial p}{\partial V}\right)_T = \frac{1}{V\kappa_T} \geqslant 0. \tag{1}$$

Here p is the pressure, V is the volume, T is the temperature, and κ_T is the isothermal compressibility. The two extremes are the liquid-vapor (minimum) and vapor-liquid (maximum) stability limits or spinodals. The first one is the stability limit for the liquid state (overheating or stretching a liquid without vaporization), while the second one is the limit of vapor state (undercooling or pressurizing a vapor without condensation). In real systems of course other stability limits exist such as for melting and crystallization[7] which cannot be modeled by the van der Waals equation of state. In the pressure-temperature plane the spinodal states lie on two distinct curves, which meet in the critical point [Fig. 1(b)]. The vapor pressure curve, representing the equilibrium conditions, lies between these two curves and meets them at the critical point. The region between the vapor pressure curve and the vapor-liquid spinodal corresponds to metastable vapor, while the region between the liquid-vapor spinodal and the vapor pressure corresponds to metastable liquid. It is interesting to note that the metastable liquid region comprehends a huge part at negative pressure. Recent detailed analysis of stability limits for pure substances and also binary mixtures based on equations of state can be found in the literature.[5,8]

As mentioned above by overheating or stretching a liquid one observes bubble nucleation well before reaching the spinodal. For this reason only the homogenous nucleation limit can be experimentally mapped, as done in the case of water, giving 593 K at atmospheric pressure and −120 MPa at room temperature.[1,2] Since the location of the spinodal cannot be measured exactly, only an estimate for technical purposes can be given and hence any method which gives a fair quantitative estimate is important.

Here we present a method for estimating the spinodal states from simulation and experimental data of the vapor-liquid interface. It should be mentioned that the complete theoretical analysis is made here for classical systems. Nonclassical effects, i.e., nonclassical diverging density fluctuations in pure fluids, are not included as they are not included in the calculation of the critical point with classical equations of state. Actually, the critical point is a special point where the stable and unstable states encounter. The nonclassical behavior at the critical point is hence also related to the behavior at the spinodal. As known from many equations of state calculations of critical states and from investigations of classical spinodals, the classical approximation is able to describe most experimental data well.

II. METHODS

A. Spinodal calculation from the interfacial properties

Unlike the solid-fluid interfaces, liquid-vapor interfaces are not sharp but rather smooth at the molecular level. The interface of many substances at low temperature far below its critical value, for example, water at room temperature, covers only a few molecules.[9,10] Approaching the critical point, it becomes wider and diverges at the critical point.[10–12] This is the case for all liquids unless thermal degradation or any other chemical reaction occurs before reaching the critical temperature.

In homogenous isotropic fluid systems the pressure tensor is constant throughout the system and its diagonal elements are equal, $p=p_{xx}=p_{yy}=p_{zz}$. The scalar pressure is related to its trace,[13–15]

$$p = \tfrac{1}{3}\mathrm{Tr}(\mathbf{p}) = \tfrac{1}{3}(p_{xx} + p_{yy} + p_{zz}). \tag{2}$$

When the system is stagnant, off-diagonal elements can be neglected and only the three diagonal elements are nonzero. In an inhomogeneous system the pressure tensor depends on the position $\mathbf{p}=\mathbf{p}(\mathbf{r})$. When the diagonal components of $\mathbf{p}$ are different and/or when the off-diagonal elements are nonzero, the pressure tensor can be written in diagonal form and decomposed in an isotropic diagonal part and a nonisotropic one. Although the trace remains unaffected to these transformations, the pressure is not defined by Eq. (2).

Let us assume a liquid film with the z-axis perpendicular to its surface and in contact with its vapor at equilibrium. The pressure component in this direction, usually called normal pressure, is constant through the interface due to the mechanical stability criterion $\nabla\cdot\mathbf{p}=0$ at equilibrium.[16] The normal pressure equals the vapor pressure of the system, $p_{zz}(z)=p_N=p_{\mathrm{vap}}$. Because of the symmetry of the system the pressure tensor components in the directions x and y are equal. They are usually called tangential pressures, $p_{xx}=p_{yy}=p_T$. The tangential pressure develops a minimum and a maximum while passing through the interface of the film, which can become even negative due to the tension in the surface. The surface tension γ is an integral over the difference between these two pressure components through the interface,[16]

$$\gamma = \int_{-\infty}^{+\infty} (p_N - p_T)dz. \tag{3}$$

While the calculation of the pressure from the average of the trace of the pressure tensor is possible in homogenous systems, it is not defined in inhomogeneous ones. Hence one cannot use Eq. (2) in an interface to get an effective pressure. As just mentioned the tangential pressure can take even negative values because the system is stabilized in an interface in equilibrium. Without the normal component acting on the interface in a three-dimensional system, a real two-dimensional system would eventually decompose at negative pressure.

So we have to calculate the present pressure at a given point in the interface as a combination of the two pressure components. We suggest, as a general approach, that the pressure can be written as a linear composition of the normal and tangential pressure,

$$p = a \cdot p_N + c \cdot p_T, \tag{4}$$

where a and c are parameters. Since the critical point belongs to the stable region, where the pressure tensor is isotropic $p=p_N=p_T$, and simultaneously to the spinodal state, the coefficients a and c satisfy the condition $a+c=1$. Hence with Eq. (4) it follows

$$p = p_N - c(p_N - p_T). \tag{5}$$

To give an idea how to obtain c we take an infinitesimal thin slice parallel to the interfacial plane. The density is uniform in the complete slice. Then we extend the infinitesimal slice on the third dimension, keeping the density and the elements of the stress tensor, which is equal to the negative pressure tensor. The stress tensor now will have two nonzero diagonal elements. To convert it to a three-dimensional system, by keeping the scalar pressure [Eq. (2)], these two nonzero elements have to be multiplied by $3/2$ to compensate the contribution of the third dimension. Therefore we get $c=3/2$ in Eq. (5). Once we have an isotropic homogenous three-dimensional phase Eq. (2) is valid again but that is not relevant for the transformation itself.

The tangential pressure component changes across the interface, reaching a minimum $p_{T,\mathrm{min}}$ somewhere inside the interface. The minimum pressure p_{min} according to Eq. (5) can then be written as

$$p_{\mathrm{min}} = p_N - c(p_N - p_{T,\mathrm{min}}). \tag{6a}$$

This is the most negative pressure that can exist in the interface. We assume here that the minimum pressure p_{min} is equal to the spinodal pressure $p_{\mathrm{sp,liq}}$. This spinodal pressure is the deepest obtainable pressure in the bulk liquid. Applying a more negative pressure one would lead to the breaking of the liquid part of the coexisting phases. We will see below that this assumption is confirmed by the results. Using this assumption, Eq. (6a) can be rewritten as

$$p_{\mathrm{sp,liq}} = p_N - c(p_N - p_{T,\mathrm{min}}). \tag{6b}$$

To complete this analysis we also apply Eq. (6b) to stable three-dimensional homogeneous states. As soon as a state is homogeneous the pressure has to be calculated from the trace of the pressure tensor which gives

$$p = \tfrac{1}{3}(p_{xx} + p_{yy} + p_{zz}) = \tfrac{1}{3}(2p_T + p_N) = p_N - \tfrac{2}{3}(p_N - p_T), \tag{7}$$

and hence by comparison with Eq. (5) we get $c=2/3$. However, this is only a formal expression because in a homogeneous phase we have $p=p_N=p_T$ and hence for stable phases including the binodal any value for c is valid. A natural choice is to take the same value as in the nonstable region. With this approach we can investigate the nonstable region with the location of the spinodal and two stable states, namely, the coexisting vapor and liquid phases.

B. Lattice Boltzmann simulations

Lattice Boltzmann simulations are performed using the original pseudopotential model of Shan and Chen (SC-LBM).[17–19] The lattice Boltzmann method (LBM) is similar to the lattice gas method with the major difference that in LBM particle groups interact instead of individual particles. In the model of Shan and Chen (SC-LBM) phase transition and phase equilibrium can be described by the application of a potential ψ that describes the interaction between the particle groups. Here the following potential is used:[17–19]

$$\psi = \rho_0(1 - e^{-\rho/\rho_0}), \tag{8}$$

where ρ is the density and ρ_0 is a constant. The corresponding equation of state is given by

$$p = \frac{c^2}{D}\left[(1-d_0)\rho + \frac{b}{2}g\psi^2\right], \tag{9}$$

where p, c, D, d_0, and b are the pressure, speed of sound, the dimension of the space of the lattice, the compressibility parameter, and the number of lattice's nodes, respectively. The variable g is the so-called fluid interaction coupling. It is interpreted as negative reciprocal temperature, $T=-1/g$. The critical value of g is $g_c=-1/9=-0.\overline{1}$.

The simulations are performed in a gravitation-free, quasi-three-dimensional system consisting of $512\times2\times2$ cells, using the three-dimensional projection of the D4Q24 lattice[20] with periodic boundary conditions. This model can describe liquid-vapor equilibrium in two and three dimensions for simple, such as argonlike systems, using sufficiently big lattices.[19,21,22] The liquid-vapor interface is perpendicular to the long axis with 512 cells. Equilibrium is reached when the density and the impulse of the two phases reached a constant value. It has been clarified earlier that reducing the other two box dimensions to two cells does not have any influence on the properties of the liquid-vapor equilibrium, including the interfacial properties.[10] However, a possible curvature of the interface cannot be studied with such setup because the interface with 2×2 cells is too small. There has been further skepticism concerning the ability of SC-LBM to describe interfaces properly.[23] That has already been addressed in an earlier work and it has been found the skepticism is not justified.[10] An exception is the thickness of the interface which can become very large, if the size of a lattice cell becomes large, for example, in the simulation of turbulences.

C. Molecular dynamics simulations

Molecular dynamics simulations of a liquid film in equilibrium with its vapor phase have been conducted with 5000 argon atoms modeled by the Lennard–Jones potential. The Lennard–Jones parameters are $\varepsilon/k_B=117.7$ K and $\sigma=0.3409$ nm. A large cut-off radius of 6.5σ is used in order to avoid significant truncation effects. We obtain stable liquid films by means of a three-step method: (a) The system is equilibrated in *NVT* ensemble starting from a homogeneous fcc crystalline configuration in a cubic box at $T=100$ K and a density of 1200 g dm^{-3}, corresponding to a liquid phase density. During this step the system melts. (b) The system is then equilibrated in *NpT* ensemble at $p=0$ bar. This step is essential for the stabilization of the film in the next step. (c) The box is expanded in one direction and the resulting film is then equilibrated in *NVT* ensemble at the final temperature of the film. In this stage some atoms evaporate while a new stationary state is reached. A simple criterion to determine whether the equilibrium has been reached is to determine the point where the mean number of atoms in the film remains constant. We define the film as the largest cluster in the system and apply the Stoddard algorithm[24] to recognize their constituent atoms. Thermal equilibrium, i.e., the temperature profile, has been checked as well. Starting from this point a production phase of 2 ns is performed at constant temperature by applying an Andersen thermostat. The simulations are performed at six temperatures from 64 to 144 K. Full periodic boundary conditions are applied in all steps and motion equations are solved by a leap-frog algorithm using an integration step equal to 1 fs.

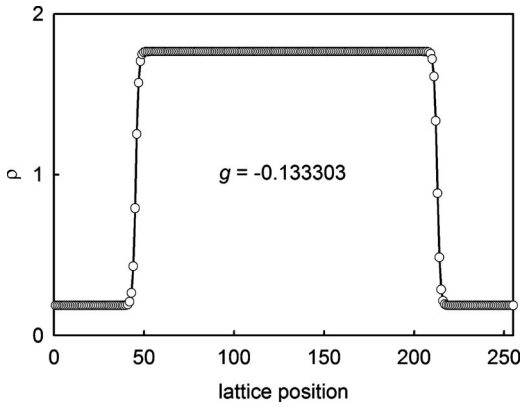

FIG. 2. Density profile of the liquid film obtained by a lattice Boltzmann simulation for $g=-0.133\,303$.

The local pressure tensor of the planar system can be written in Cartesian coordinates as

$$\mathbf{p}(z) = (\mathbf{e}_x\mathbf{e}_x + \mathbf{e}_y\mathbf{e}_y)p_T(z) + \mathbf{e}_z\mathbf{e}_z p_N(z), \tag{10}$$

where p_N and p_T are, respectively, the normal and tangential components of the pressure tensor. We use here the formulation of Irving–Kirkwood[25] for the calculation of the tangential pressure components: all pairs connected by a line crossing the chosen z-plane contribute to the configuration part of the pressure components in the plane z. Thus the tangential and normal local pressure are given by

$$p_N(z) = \rho(z)k_BT - \frac{1}{2A}\left\langle \sum_{i\neq j} |z_{ij}| \frac{1}{r_{ij}}\frac{\partial U}{\partial r_{ij}}\Theta\left(\frac{z-z_i}{z_{ij}}\right)\Theta\left(\frac{z_j-z}{z_{ij}}\right)\right\rangle, \tag{11}$$

$$p_T(z) = \rho(z)k_BT - \frac{1}{4A}\left\langle \sum_{i\neq j} \frac{x_{ij}^2+y_{ij}^2}{|z_{ij}|} \frac{1}{r_{ij}}\frac{\partial U}{\partial r_{ij}}\Theta\left(\frac{z-z_i}{z_{ij}}\right)\Theta\left(\frac{z_j-z}{z_{ij}}\right)\right\rangle, \tag{12}$$

where $\Theta(x)$ is the Heaviside function defined as $\Theta(x)=1$ for $x>0$ and 0 otherwise.

III. RESULTS

A. Lattice Boltzmann simulations

A typical lattice position versus density plot obtained from the SC-LBM simulation is shown in Fig. 2. A liquid film in the simulation box is surrounded by vapor. The value for g is $-0.133\,303$, the liquid and vapor equilibrium densities are 1.77 and 0.19, respectively. Using the 10–90 interface definition, i.e., the interface is defined as the part, where the density is smaller than $\rho_1-0.9(\rho_1-\rho_v)$ and larger than $\rho_v+0.1(\rho_1-\rho_v)$, the interface thickness is nine lattice units. According to a previous study,[10] this corresponds to approxi-

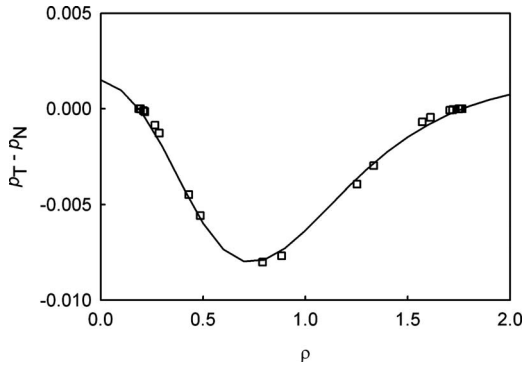

FIG. 3. Plot of the tangential and normal pressure components difference as function of the density. The symbols are results of the LBM simulation, the solid curve is the correlation with Eq. (13).

mately 3.6 nm or roughly nine atoms, if compared to atomistic simulations for argon. The density profile in the interface can be properly described with a tangent hyperbolic function,[10] as expected for a mean field model.[26,27]

The difference of the pressure components in the interfacial region is shown in Fig. 3. Instead of plotting $p_T - p_N$ versus the lattice position we plot it against the density through the interface. Since the simulated liquid film has two interfaces we obtain twice the number of data points for the interface. In order to estimate the minimum pressure the data points are approximated by a correlation function

$$f = B - A \exp\left(-\exp\left(-\frac{\rho - C}{D}\right) - \frac{\rho - C}{D} + 1\right), \tag{13}$$

with the parameters $A=0.009\,73$, $B=0.001\,72$, $C=0.737\,51$, and $W=0.386\,38$ for $g=-0.133\,303$. The minimal pressure difference $p_{T,\min} - p_N$ is calculated as the minimum of the correlation function.

In Fig. 4 the comparison of the spinodal directly calculated from the LBM equation of state [Eq. (13)] and spinodal estimated from the interfacial simulation data using Eq. (6b) is shown. Obviously the agreement is very good, within the error of the determination of the pressure minimum. The error increases as the surface thickness decreases; this is due to the decrease of the number of data points (i.e., the number of particles) used to describe a continuous interface. This agreement supports our assumption concerning the connection of surface tension and spinodal and it also supports the validity of Eq. (6b). The determination of the vapor spinodal as described below for molecular simulations was not possible for the LBM simulations performed here. The resolution of the LBM is not high enough to describe small regions of the interface as the maximum of tangential pressure. Therefore we have omitted the estimation of the vapor spinodal from the LBM simulations here. In the next section we analyze the relation between the interfacial tangential pressure and the spinodals with molecular dynamics simulation.

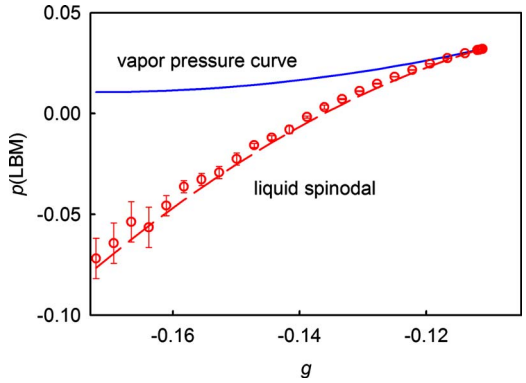

FIG. 4. (Color online) Pressure-g plot of the vapor pressure curve and the liquid spinodal calculated from the LBM equation of state [Eq. (9)] and the spinodal estimated form the interfacial tension using $c=3/2$.

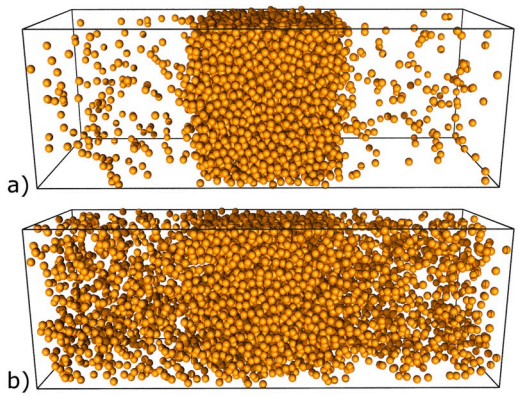

FIG. 5. (Color online) Snapshots of the equilibrated argon liquid film simulations at (a) 112 K and (b) 144 K.

B. Molecular dynamics simulations

1. Analysis and correlation of the simulation data

We performed molecular dynamics simulation of liquid film in equilibrium with the vapor phase for Lennard–Jones argon with a similar setup as for the LBM simulations. In a rectangular box the film is placed in the middle as shown in the snapshots in Fig. 5. In total we have chosen six temperatures. At 112 K significantly below the critical temperature one can clearly distinct between the vapor phase and the liquid film. Closer to the critical point at 144 K liquid and vapor densities approach each other and the interface becomes wider and diffuse.

The profiles of the density, of the normal, and of the tangential pressure are plotted for 96 K in Fig. 6. All profiles are fitted to analytical functions. The density profile is fitted to a commonly used expression[28,29] given by

$$\rho(z) = 0.5(\rho_1 + \rho_v) - 0.5(\rho_1 - \rho_v)\tanh\left(\frac{2(z-l)}{d}\right). \tag{14}$$

The parameters of this function have physical meaning: l and d are the thickness of the film and the interface, respectively, and ρ_l and ρ_v are the densities of the liquid and vapor bulk phases. The parameters of the functions for all five temperatures chosen here are listed in Table I.

The normal pressure is decomposed in two terms: a kinetic positive term and a negative configuration part,

$$p_N(z) = p_N^K(z) + p_N^{IJ}(z). \tag{15}$$

Here the kinetic part is fitted by the expression

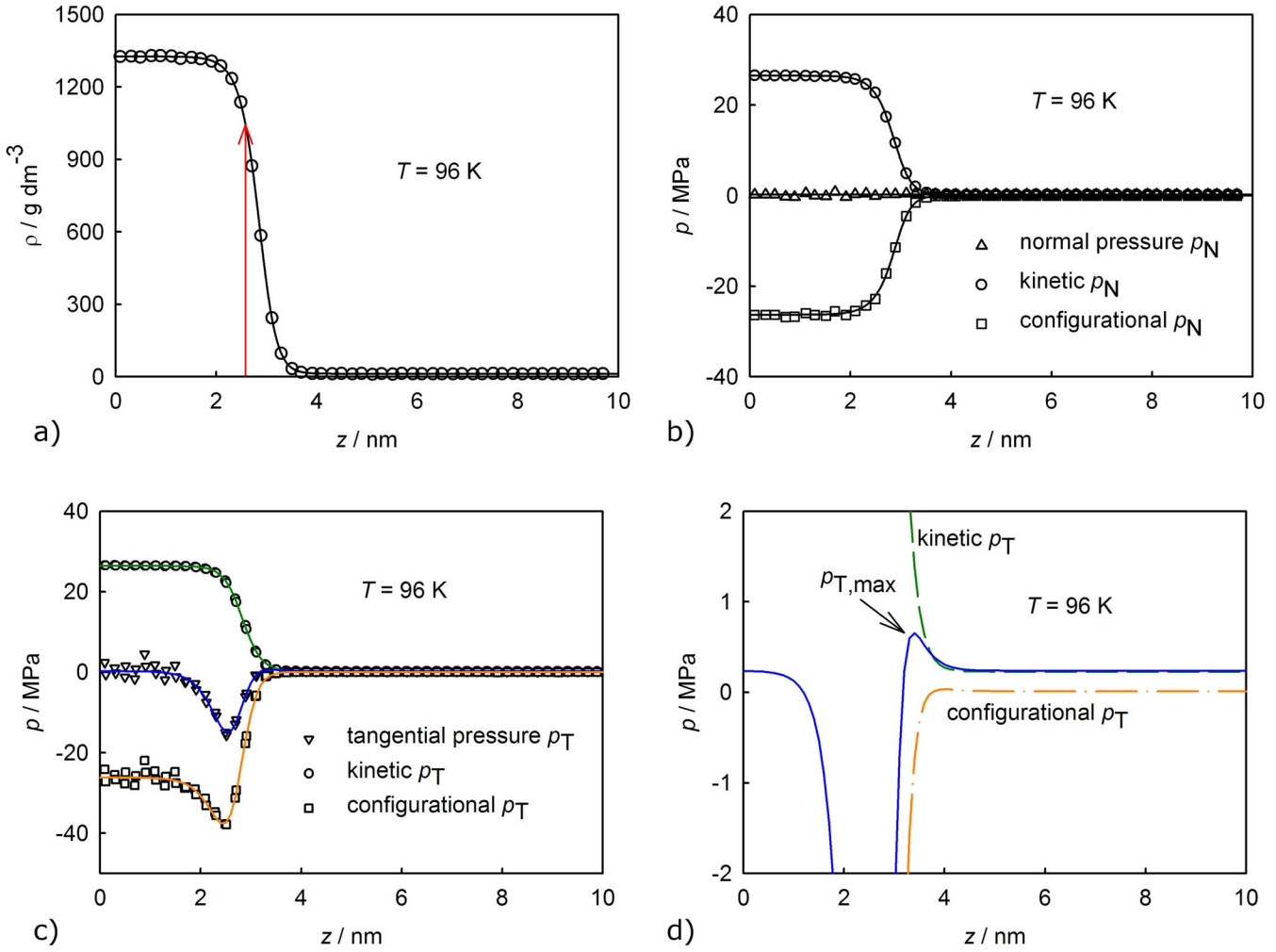

FIG. 6. (Color online) Pressure and density profiles across an interface at 96 K. (a) Density profile. (b) Normal pressure profile. (c) Tangential pressure profile. For the pressure profiles the kinetic and the potential contributions are added. The minimum in (c) corresponds to the density marked by an arrow in (a). (d) Tangential pressure profile perpendicular to the interface enlarged near the maximum on the vapor side.

$$p_N^K(z) = 0.5(p_{N,1}^K + p_{N,v}^K) - 0.5(p_{N,1}^K - p_{N,v}^K)\tanh\left(\frac{2(z-l)}{d}\right) \equiv f_1(z) \tag{16}$$

where $p_{N,l}^K$ and $p_{N,v}^K$ are the kinetic contributions of the normal pressure in the liquid and vapor bulk phases. The parameters are listed in Table II. Since the normal pressure is constant $p_N(z)=p_N$, which is the mechanical constant pressure condition for phase equilibrium, the virial part of the normal pressure is adjusted as

$$p_N^U(z) = p_N - p_K^U(z). \tag{17}$$

As it was already mentioned p_N is also equal to the vapor pressure at the temperature of the system. The tangential pressure can also be decomposed in two terms: a kinetic positive term and a virial negative one.

$$p_T(z) = p_T^K(z) + p_T^U(z). \tag{18}$$

The difference between the normal and tangential pressures is fitted with the function proposed by Fuchs,[30]

$$p_N(z) - p_T(z) = q(\rho(z)\rho''(z) - [\rho'(z)]^2) \equiv f_2(z), \tag{19}$$

with a parameter q. Inserting the fitted tangent hyperbolic function of the density profile into Eq. (19) we obtain

TABLE I. Parameters of the correlation function [Eq. (14)] for the density profiles.

	64 K	80 K	96 K	112 K	128 K	144 K
ρ_l (g dm^{-3})	1512.78	1420.46	1321.91	1214.35	1079.34	885.628
ρ_v (g dm^{-3})	0	1.550 39	11.198 6	35.473	87.319 6	204.302
l (nm)	2.922 34	2.682 34	2.831 76	2.940 68	3.125 29	2.826 28
d (nm)	0.442 27	0.567 86	0.741 90	0.964 67	1.352 87	2.438 87
r^2	0.999 75	0.999 83	0.999 91	0.999 93	0.999 90	0.999 70

TABLE II. Parameters for the correlation function [Eq. (16)] for the kinetic part of the normal and the tangential pressure.

	64 K	80 K	96 K	112 K	128 K	144 K
$p_{N,l}^K$ (MPa)	20.150 8	23.629 91	26.403 79	28.213 11	28.709 99	26.509 65
$p_{N,v}^K$ (MPa)	0	0.029 638	0.227 01	0.863 91	2.349 61	6.120 80
l (nm)	2.920 46	2.683 62	2.831 86	2.941 31	3.124 51	2.831 92
d (nm)	0.439 69	0.566 39	0.741 95	0.962 21	1.353 48	2.433 81
r^2	0.999 73	0.999 81	0.999 91	0.999 94	0.999 92	0.999 71

$$f_2(z) = \mathrm{sech}^2(Z)[(a-b)(1+\tanh^2(Z)) - 2(a+b)\tanh(Z)], \tag{20}$$

with $Z=2(z-h)/d$. The parameters for this correlation function are listed in Table III. Because of the isotropy of the kinetic part of the pressure, equation $p_T^K(z)=p_N^K(z)$ is satisfied and then the virial part of the tangential pressure is $p_T^U(z)=p_N^U(z)-f_2(z)$ and the tangential pressure is $p_T(z)=p_N(z)-f_2(z)$. With this selection of the fitting functions the following conditions are fulfilled: (a) the normal pressure is constant along the axis z, (b) the kinetic parts of the tangential and the normal pressure are equal, (c) the difference between the tangential and normal pressure vanishes as the liquid and vapor bulk phases are approached, (d) the tangential pressure profile exhibits a minimum and a maximum corresponding to the liquid and vapor spinodal pressures, respectively. These conditions assure the convergence of the integral [Eq. (3)] and give a good agreement for the surface tension.[31]

2. Estimation of the spinodals

To estimate the spinodal from the simulation data of the interface we have transformed the tangential pressure profile from the z-coordinate dependence $p_T(z)$ to the density dependence $p_T(\rho)$ using the interfacial density profile $\rho(z)$. This transformation is shown in Fig. 6 in detail. In Fig. 7 the simulation data are plotted together with the correlation function given above which are transformed in the same way as the data itself. The curves resemble that of the well known a der Waals loop illustrated in Fig. 1(a) for the van der Waals equation of state. In order to compare these curves quantitatively with the equations of state developed for the Lennard–Jones fluid, we transformed the isotherms calculated from the equations of state to the scale of the tangential pressure component by inverting Eq. (5),

$$p_T = p_{\mathrm{vap}} - \frac{1}{c}(p_{\mathrm{eos}} - p_{\mathrm{vap}}). \tag{21}$$

Figure 7(a) shows the transformation of the equation of state of Kolafa and Nezbeda[32] (KN) and that of Quiñones-Cisneros and Deiters[33] (QCD) using $c=3/2$ for both. One can see that the curves are qualitatively similar but there is a quantitative difference. This difference is not surprising because these Lennard–Jones equations of state are developed as most other equations of state for the stable phase region and no data of the nonstable (metastable and unstable) regions are included. It is therefore a prediction and in this context can be regarded as reasonable representation of the simulation data. In other words the simulation of the interface gives additional information for the nonstable region where equation of state can give extrapolations only.

To estimate the liquid spinodal we have calculated the minimum of the tangential pressure from the correlation functions of the interfacial properties. The simulation results for the spinodal density and the corresponding tangential pressure maxima for all six temperatures and the vapor pressure are listed in Table IV. The minimum for 96 K is marked by the arrow in Fig. 6(c). The corresponding density at the same z-value is marked by an arrow in Fig. 6(a). In this way we obtain the liquid spinodal in the density-temperature projection. As shown in Fig. 8(a) the spinodal agrees very well with that calculated from the KN equation of state.

The liquid spinodal pressure is calculated from the tangential pressure minima using Eq. (6b). The resulting values for the liquid spinodal are plotted in Figs. 8(b) and 8(c) and compared to calculations with the KN equation of state. One can see that the agreement is very good. The deviation of the spinodal obtained from the simulation to the spinodal of the equation of state is similar to that of the two binodals. It has been already pointed out earlier that for suitable equations of state the spinodal follows changes in the binodal.[5]

The estimation of the vapor spinodal is more difficult

TABLE III. Parameters for the correlation function [Eq. (20)] for the difference between the configuration parts of the normal and tangential pressure.

	64 K	80 K	96 K	112 K	128 K	144 K
a (MPa)	8.147 48	14.283 3	9.047 33	4.999 12	2.295 92	0.532 62
b (MPa)	−21.147 5	0.803 53	0.469 94	0.494 20	0.488 67	0.320 53
h (nm)	2.564 03	2.682 32	2.823 96	2.941 1	3.107 25	2.673 32
d (nm)	0.525 95	0.868 13	1.016 95	1.211 17	1.542 54	2.957 7
r^2	0.998 10	0.977 26	0.954 24	0.934 33	0.791 06	0.447 6

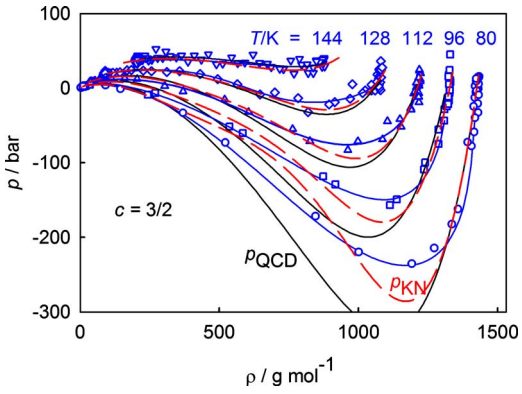

FIG. 7. (Color online) Plot of the tangential pressure vs the density. The symbols are the simulation data of the interface transformed to this projection via the density profile. The solid curves passing through the data points are calculated directly from the correlation functions of the pressure components $p_N(z)$, $f_1(z)$, and $f_2(z)$. The dashed curves marked by p_{KN} are the isotherms calculated from the KN equation of state and the solid curves marked by p_{QCD} are the isotherms calculated from the QCD equation of state. (a) Equation of state curves are transformed with Eq. (21) to p_T using $c=3/2$.

because the tangential pressure maximum is rather flat if plotted as function of the density. However, the physically based correlation functions for the pressure components and the density profile listed above allow a reasonable estimation of the vapor spinodal even in the $p_T(z)$ plot. In Fig. 6(d) this maximum is enlarged in a $p_T(z)$ plot. The vapor spinodal is calculated from the simulation data by

$$p_{sp,vap} = p_N - c(p_N - p_{T,max}). \tag{22}$$

As one can see in Fig. 8 that the vapor spinodal also agrees with the calculations using the KN equation of state. There are some deviations for the data points at 144 K which are related to the fact that this simulation is inaccurate due to finite size effect. Furthermore, the simulation data for 144 K are extremely flat which makes the estimation of the extremes inaccurate. The deviation of the data point at 80 K for the vapor spinodal is an uncertainty of the correlation function. At low temperature the peak corresponding to the maximum in the excess pressure profile is very small in comparison to the deep minimum peak. Therefore any global fitting of the data leads to a poor description of the maximum and hence of the vapor spinodal. In order to improve the determination of the vapor spinodal, we have applied a local fit in the vicinity of the pressure maximum only. The maximum pressure obtained in this way is more accurate, as one can see in Fig. 8 (open diamonds). Hence, we find good agreement between the interfacial tangential pressure and the spinodal obtained from the simulations and the equation of state. This result therefore justifies our approach of the estimation of the spinodal with Eqs. (5), (6a), and (6b).

C. Analysis of the experimental data

We present here a simple method to estimate the liquid spinodal pressure from experimental equilibrium interfacial data, surface tension, and interfacial thickness. The method involves the assumption of the algebraic form of the tangential pressure profile. As a first approach, which we call rectangle approximation here, we assume an interface with the thickness d where the tangential pressure is uniform and equal to $p_{T,min}$. This rather simple rectangle approximation gives a thumb rule for estimating liquid spinodal pressures. Within this assumption the maximum on the vapor side is neglected. The normal pressure is equal to the vapor pressure. Therefore the surface tension given by Eq. (3) changes

TABLE IV. Vapor pressure or normal pressure, densities, pressure, and z-coordinate at the maxima and minima of the tangential pressure. The data are obtained from the correlation functions Eqs. (14), (16), and (20). The numbers in brackets are obtained from a local fit in the vicinity of the vapor density, vapor pressure, and pressures maximum and minimum.

	64 K	80 K	96 K	112 K	128 K	144 K
p_N (MPa)	0 (0.002 866)	0.053 042	0.237 99	0.756 10	1.823 97	3.707 02
ρ_l (g dm^{-3})	1512.78	1420.46	1321.91	1214.35	1079.34	885.628
ρ_v (g dm^{-3})	0 (0.25)	1.550 39	11.1986	35.473	87.3196	204.302
z_{min} (nm)	2.690 39	2.440 35	2.540 82	2.599 92	2.661 15	1.7533
z_{max} (nm)	3.38	3.154 76	3.385 63	3.533 87	3.760 05	3.7191
$\rho_{l,sp}$ (g dm^{-3})	1347.3 (1270)	1202.13	1095.93	983.568	878.703	785.598
$\rho_{v,sp}$ (g dm^{-3})	22.7113 (44.14)	50.6885 (66.51)	74.1834 (99.94)	128.292 (152.53)	219.017	332.259
$p_{T,max}$ (Mpa)	0.2 (0.271)	0.784 89 (0.3938)	0.65591 (0.7884)	1.281 62 (1.3103)	2.439 58	4.177 84
$p_{T,min}$ (Mpa)	−37.4252 (−34)	−23.9019	−14.9426	−7.589 86	−1.964 07	2.859 73

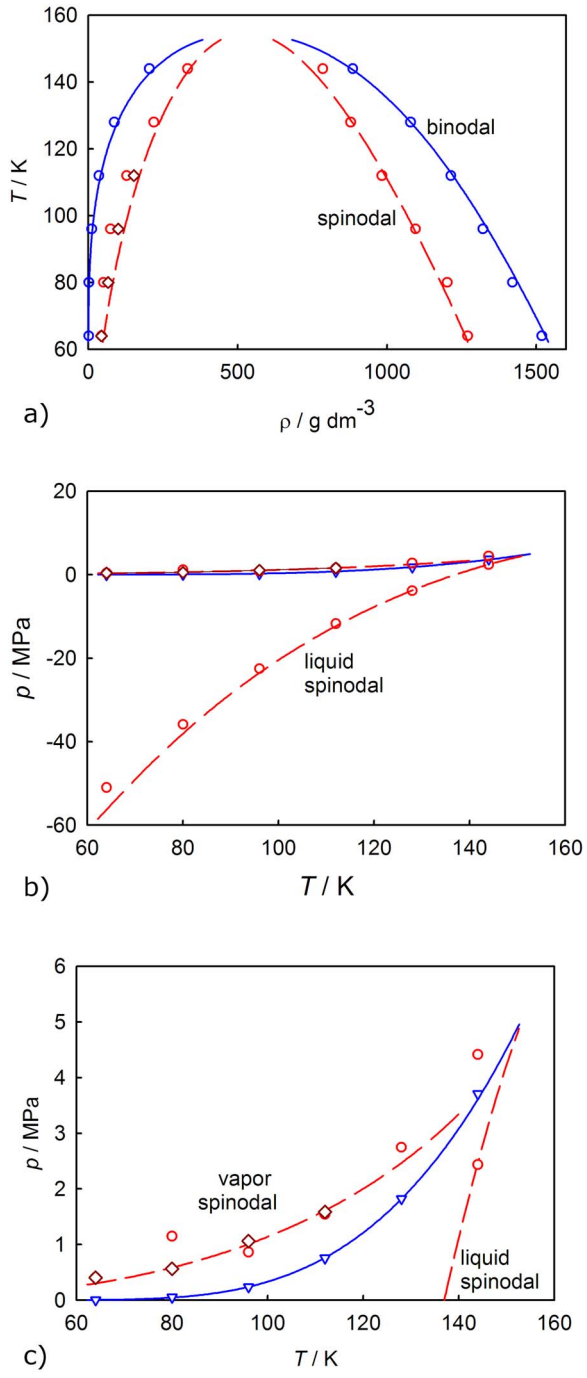

FIG. 8. (Color online) Comparison of the simulation data (symbols) to the calculations with the KN equation of state (curves) for the binodal and the spinodal. (a) Temperature-density projection. (b) Pressure-temperature projection. (c) Enlargement of the pressure-temperature projection at positive pressure. In all diagrams the open diamonds on the vapor side are the spinodal data obtained from local fit of the pressure maximum on the vapor side.

to $\gamma = d \cdot (p_{\mathrm{vap}} - p_{T,\mathrm{min}})$. The minimum tangential pressure obtained from the last equation is then replaced in the transformation with Eq. (6b) to get the spinodal liquid pressure. In a second approach we describe the interfacial profiles with Eqs. (14) and (19). We insert a dimensionless form of the hyperbolic-tangent density profile [Eq. (14)] $\rho(z) = 1 - B \tanh(2z/d)$ into Eq. (19) for the excess pressure profile. The parameter $B = (\rho_l - \rho_v)(\rho_l + \rho_v)^{-1}$ is close to unity at low and moderate temperatures where the equilibrium liquid density is much larger than the vapor density. Equation (3) is used to obtain the analytical form of the excess pressure profile from which, according to Eq. (6b), the liquid spinodal pressure can be calculated.

Both approximations are used to estimate the liquid spinodal of two fluids, namely, water and helium-4. The spinodals are widely studied for these two systems (see, for example, references in Ref. 2) and the surface tension and interface thickness data are also available. Inserting $\gamma = d \cdot (p_{\mathrm{vap}} - p_{T,\mathrm{min}})$ in Eq. (6b) gives the expression for the spinodal pressure within the rectangle approximation,

$$p_{\mathrm{sp,liq}} = p_{\mathrm{vap}} - c\frac{\gamma}{d}, \tag{23}$$

where c is taken as 3/2. The vapor pressure for helium-4 at 1.2 K is practically zero [10^{-4} MPa, as given by the International Temperature Scale of 1990 (Ref. 34) for 1.23 K]. The surface tension is 0.000 36 N/m and the interfacial thickness is $d = 7 \times 10^{-10}$ m.[35,36] In this way, $p_{T,\mathrm{min}}$ is −0.51 MPa. The calculated surface spinodal with rectangle-approximation approximation turns out to be around −0.77 MPa, which is close to the deepest measured value of −0.80 MPa.[2]

The surface tension of water at 298.15 K is much higher, namely, 7.4×10^{-2} N/m, while the surface thickness is still in the same order of magnitude, being $d = 3.2 \times 10^{-10}$ m.[9] The vapor pressure is relatively low, 3×10^{-3} MPa. This gives a peak pressure of around −230 MPa and a spinodal pressure of about −350 MPa. For water, there are two models, one—mainly proposed by Speedy—which states that the spinodal has a limit around room temperature (reentrant spinodal), while the other—originated from Skripov—states that it decreases monotonously with the temperature.[1,2,37–40] The latter one gives twice as deep value for the spinodal at room temperature than the reentrant one (−400 versus −200 MPa). This −350 MPa lies between the reentrant and the Skripov model.[1,2] To verify any of these two models by our method, the extension of surface tension,[41] the interfacial thickness, and the constant c from Eq. (21) into the region of metastable vapor-liquid equilibrium states will be necessary. Such studies are in progress.

The second approximation gives for helium-4 at 1.2 K a minimum tangential pressure of −0.6508 MPa and a liquid spinodal pressure of −0.9762 MPa. For water minimum tangential pressure is −292.7 MPa and the liquid spinodal pressure is −439 MPa. In both cases the spinodal pressure takes a somewhat larger negative value than the predictions of the rectangle approximation and the experimental values. This result is consistent with the fact that any metastable liquid would cavitate before it reaches the spinodal state. On the other hand, the minimum tangential pressure and consequently the liquid spinodal pressure obtained by the rectangle approximation represent a conservative estimation since the minimum tangential pressure corresponds to the mean value of the integral of a more realistic local pressure profile. In order to account for deviations from the rectangular approximation one can introduce an effective shape factor s in Eq. (23) giving

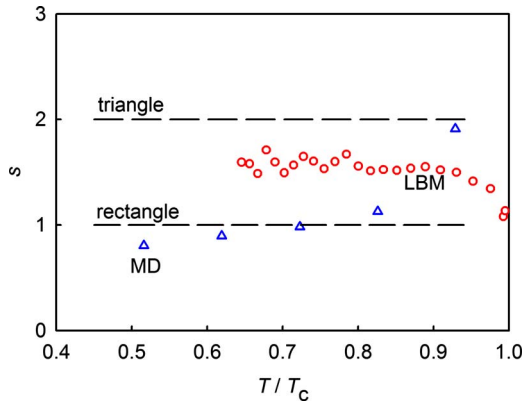

FIG. 9. (Color online) Shape factor s calculated from the simulation data and plotted vs the reduced temperature. The shape factors for a rectangle and a triangle are marked by dashed lines. Triangles: MD data; circles: LBM data.

$$p_{\mathrm{sp,liq}} = p_{\mathrm{vap}} - s \cdot c\frac{\gamma}{d}. \tag{24}$$

This effective shape factor s is equal to 1 if we assume a rectangular shape of the peak and 2 for a triangular shape. It should be made very clear that this does not mean that the peak is actually rectangular or triangular, it just means that it can effectively described by such shapes. In Fig. 9 the shape factor calculated with rearranged Eq. (24) using the simulation data of surface tension, interfacial thickness, and liquid spinodal pressure is plotted for the molecular dynamics (MD) and LBM simulations performed here. This diagram gives an idea about realistic values for the shape factor because we can use the consistent data sets obtained from the simulation including all properties required in Eq. (24) and the liquid spinodal pressure calculated from Eq. (6b). As discussed above the rectangular shape appears to be a lower limit, while the triangle is like an upper border. Interestingly the shape factors up to $T/T_c=0.9$ are roughly 1 for MD and 1.5 for LBM. The notorious increase of the shape factor close to the critical temperature, $T/T_c=0.9$, is likely related to the fact that the positive and negative contributions to the interfacial tension become comparable at higher temperature. At low temperature this compensation effect is negligible since the negative contribution corresponding to the minimum of the excess pressure profile dominates by far over the positive one. The shape factors obtained from MD and LBM simulations exhibit also different critical behaviors. While the shape factor of the MD simulations appears to diverge to positive values, the LBM shape factors tend to the value zero. An analysis of the exponents of the power laws for d, γ, and $p_{\mathrm{vap}}-p_{\mathrm{sp,liq}}$ gives an exponent for s of -0.61 in the case of MD simulations and 0.07 for LBM simulations.

We also should mention here, that using this method, the prediction gives back the proper limiting behavior of the spinodal pressure at the critical point because surface tension goes to zero and interface thickness diverges, giving zero peak excess pressure.

IV. SUMMARY AND CONCLUSION

The results gathered in this investigation are manifold. First, it appears that the interfacial tangential pressure plotted versus the interfacial density gives a van der Waals loop in the nonstable region as suggested by the van der Waals equation of state. Many equations of state exhibit this loop while there are also several equations, typically highly accurate many-parameter correlation equations, which have more extremes in the two-phase region or even discontinuous behavior. This is usually the result of highly accurate correlation of the experimental data in the stable region of the phase diagram forcing all undesired mathematical behavior into the nonstable region. The interfacial continuity as obtained form simulations is therefore useful for the development of equations of state suitable for metastable systems.

There is a long discussion about the extension of equations of state into the nonstable (i.e., metastable and unstable) region.[42] Hill,[43] for example, has proposed to directly use the van der Waals equation of state for the tangential pressure in Eq. (3). While it is generally accepted to extrapolate an isotherm into the metastable region, it is criticized that a system cannot exist at the unstable branch of the isotherm.[44] There is no doubt that a three-dimensional homogeneous system cannot exist in the unstable region but by crossing an interface one passes trough local states where the mechanical stability condition of a uniform systems is not satisfied. A two-phase system forms an interface where the density evolves continuously. A sharp interface would give vanishing surface tension according to Eq. (3). If one continuously varies the density at a constant subcritical temperature, one has to pass through the unstable region in the phase diagram as well as in the interface. The mechanical stability criterion requires that the normal pressure is constant through the interface. Therefore only the tangential components can take the values which correspond to the density in the unstable region. This consequently leads also to $c=3/2$ in Eqs. (5), (6a), and (6b).

Furthermore, the value $c=3/2$ in Eq. (5) leads to a definition of the local pressure in a planar inhomogeneous system. Mareschal *et al.*[45] presented an ensemble-averaged definition of the local pressure where the configuration part only includes the contribution of pairs located in a two-dimensional plane. For practical application a coarse-grained approximation of the local pressure is introduced where a thin three-dimensional slab is used instead of a two-dimensional system.[46–48] In ongoing investigations we further analyze the relation between our local pressure definition given by Eq. (5) and other approaches.

We show here that the classical spinodal can be directly estimated by microscopic and mesoscopic equilibrium simulations of liquid-vapor interfaces. This is a comparable simple way for the estimation of a spinodal besides the binodal directly from an equilibrium simulation. Furthermore, one can apply the corresponding state principle to compare the results of the interfacial thickness obtained by LBM and MD simulations. The reduced temperature of LBM system is $T_r=g/g_c$, which takes the value of 0.8335 for $g=-0.133\,303$. This reduced temperature corresponds approximately to the simulation of LJ-argon at 128 K. For this system the interfacial thickness is 1.35 nm and even smaller if the 10-90 definition is applied as for the analysis of the LBM simulations. This value is about 2.7 times smaller com-

pared to the LBM result being 3.6 nm as mentioned in Sec. III A. Hence, although it is difficult to determine the interface exactly it is possible to link the liquid spinodal pressure to the minimum of the tangential pressure component with the same c value as for molecular simulations. This supports the generality of the approach presented here. It is apparently not restricted to a particular type of interaction.

Finally, based on this analysis of the interface simulations we propose a simple approximation to estimate the liquid spinodal pressure from experimental data of the surface tension and interfacial thickness given by Eq. (23). This method can be useful for spinodal estimation especially in systems where qualitative deviations from the usual monotonic behavior are expected such as water.

ACKNOWLEDGMENTS

The authors wish to explain their thanks to Professor H. Morgner (Leipzig) and for Dr. F. Caupin (Paris) for their helpful advices. This work is partly supported by the Hungarian Academy of Science (HAS) and the German Research Foundation (DFG) within joint project 436 UNG 113/150. R.R. has received a Ph.D. fellowship by the German exchange service (DAAD). A.R.I. stay in Germany was supported by the German Humboldt Foundation. Further supports by the DFG (KR1598/19-2), OTKA (K67930) and Bolyai Research Grant are acknowledged.

[1] P. G. Debenedetti, *Metastable Liquids: Concepts and Principles* (Princeton University Press, Princeton, 1996).
[2] *Liquids Under Negative Pressures*, edited by A. R. Imre, H. J. Maris, and P. R. Williams, NATO Science Series II (Kluwer, Dordrecht, 2002), Vol. 84.
[3] D. H. Trevena, *Cavitation and Tension in Liquids* (Adam Hilger, Bristol, 1987).
[4] E. Roedder, Science **166**, 1413 (1967).
[5] T. Kraska, Ind. Eng. Chem. Res. **43**, 6313 (2004).
[6] I. Polishuk, R. González, J. H. Vera, and H. Segura, Phys. Chem. Chem. Phys. **6**, 5189 (2004).
[7] A. R. Imre, A. Drozd-Rzoska, Á. Horváth, T. Kraska, and S. J. Rzoska, "Solid-fluid phase transtions under extreme pressures including negative ones," J. Non-Cryst. Solids (submitted).
[8] A. R. Imre and T. Kraska, J. Chem. Phys. **122**, 064507 (2005).
[9] L. X. Dang and T. M. Chang, J. Chem. Phys. **106**, 8149 (1997).
[10] G. Mayer, G. Házi, J. Páles, A. R. Imre, B. Fischer, and T. Kraska, Int. J. Mod. Phys. C **15**, 1049 (2004).
[11] C. Croxton, *Introduction to Liquid State Physics* (Wiley, London, 1975).
[12] V. K. Shen and P. G. Debenedetti, J. Chem. Phys. **114**, 4149 (2001).
[13] C. Truesdell and C.-C. Wang, *Rational Thermodynamics*, 2nd ed. (Springer, New York, 1984).
[14] R. B. Bird, W. E. Stewart, and E. N. Lightfoot, *Transport Phenomena*, 2nd ed. (Wiley, New York, 2002).
[15] S. Hess, in *Lecture Notes in Physics 381, Rheological Modelling: Thermodynamical and Statistical Approaches*, edited by J. Casas-Vasquez and D. Jou (Springer-Verlag, Berlin, 1991), p. 51.
[16] J. S. Rowlinson and B. Widom, *Molecular Theory of Capillarity* (Dover, New York, 2003).
[17] X. Shan and H. Chen, Phys. Rev. E **47**, 1815 (1992).
[18] X. Shan and H. Chen, Phys. Rev. E **49**, 2941 (1993).
[19] Y. H. Qian and S. H. Chen, Int. J. Mod. Phys. C **8**, 763 (1997).
[20] N. S. Martys and S. Chen, Phys. Rev. E **53**, 743 (1996).
[21] A. R. Imre and G. Házi, Int. J. Mod. Phys. C **13**, 649 (2002).
[22] G. Mayer, G. Házi, A. R. Imre, T. Kraska, and L. V. Yelash, Int. J. Mod. Phys. C **15**, 459 (2004).
[23] X. He and G. D. Doolen, J. Stat. Phys. **107**, 309 (2002).
[24] S. D. Stoddard, J. Comput. Phys. **27**, 291 (1978).
[25] J. H. Irving, J. G. Kirkwood, J. Chem. Phys. **18**, 817 (1950).
[26] F. P. Buff, R. A. Lovett, and F. H. Stillinger, Phys. Rev. Lett. **15**, 621 (1965).
[27] M. Hasenbusch, Int. J. Mod. Phys. C **12**, 911 (2001).
[28] C. A. Leng, J. S. Rowlinson, and S. M. Thompson, Proc. R. Soc. London, Ser. A **352**, 1 (1976).
[29] S. M. Thompson, K. E. Gubbins, J. P. B. R. Walton, R. A. R. Chantry, and J. S. Rowlinson, J. Chem. Phys. **81**, 530 (1984).
[30] K. Fuchs, Repertorium der Physik **24**, 141 (1888).
[31] M. Mecke, J. Winkelmann, and J. Fischer, J. Chem. Phys. **107**, 9264 (1997).
[32] J. Kolafa and I. Nezbeda, Fluid Phase Equilib. **100**, 1 (1994).
[33] S. E. Quiñones-Cisneros, U. K Deiters, Presentation at Thermodynamics 2005, Sesimbra, Portugal (unpublished).
[34] International Temperature Scale of 1990 (ITS-90), see, for example, http://www.bipm.org.
[35] C. Vicente, W. Yao, H. J. Maris, and G. M. Seidel, Phys. Rev. B **66**, 214504 (2002).
[36] K. Penanen, M. Fukuto, R. K. Heilmann, I. F. Silvera, and P. S. Pershan, Phys. Rev. B **62**, 9621 (2000).
[37] P. H. Poole, F. Sciortino, U. Essmann, and H. E. Stanley, Phys. Rev. E **48**, 3799 (1993).
[38] P. G. Debenedetti, J. Phys.: Condens. Matter **15**, R1669 (2003).
[39] R. J. Speedy, J. Phys.: Condens. Matter **16**, 6811 (2004).
[40] P. G. Debenedetti, J. Phys.: Condens. Matter **16**, 6815 (2004).
[41] V. G. Baidakov, S. P. Protsenki, Z. R. Kozlova, and G. G. Chernyk, J. Chem. Phys. **126**, 214505 (2007).
[42] H. Metiu and E. Ruckenstein, AIChE J. **17**, 226 (1971).
[43] T. L. Hill, J. Chem. Phys. **20**, 141 (1952).
[44] B. Widom, J. Chem. Phys. **43**, 3892 (1965).
[45] M. Mareschal, M. Baus, and R. Lovett, J. Chem. Phys. **106**, 645 (1997).
[46] R. Lovett and M. Baus, J. Chem. Phys. **106**, 635 (1997).
[47] H. El Bardouni, M. Mareschal, R. Lovett, and M. Baus, J. Chem. Phys. **113**, 9804 (2000).
[48] H. Heinz, W. Pauli, and K. Binder, Phys. Rev. E **72**, 066704 (2005).